ION IMPLANTATION FOR HIGH PERFORMANCE III-V JFETS AND HFETS

J. C. Zolper, A. G. Baca, M. E. Sherwin[a], and J. F. Klem
Sandia National Laboratories, Albuquerque, NM 87185-0603
[a] present address: Microwave Signal, Inc., 22300 COMSAT Dr., Clarksburg, MD 20871

ABSTRACT

Ion implantation has been an enabling technology for the realization of many high performance electronic devices in III-V semiconductor materials. We report on advances in ion implantation processing technology for application to GaAs JFETs, AlGaAs/GaAs HFETs, and InGaP or InAlP-barrier HFETs. In particular, the GaAs JFET has required the development of shallow p-type implants using Zn or Cd with junction depths down to 35 nm after the activation anneal. Implant activation and ionization issues for AlGaAs will be reported along with those for InGaP and InAlP. A comprehensive treatment of Si-implant doping of AlGaAs is given based on the donor ionization energies and conduction band density-of-states dependence on Al-composition. Si and Si+P implants in InGaP are shown to achieve higher electron concentrations than for similar implants in AlGaAs due to the absence of the deep donor (DX) level. An optimized P co-implantation scheme in InGaP is shown to increase the implanted donor saturation level by 65%.

INTRODUCTION

Ion implantation has been widely used in electronic and photonic devices based on compound semiconductors. Generally, the implantation process serves one of three functions. First, selective area implant doping is used to form low resistance contact regions in Field Effect Transistors (FETs), Heterojunction Bipolar transistors (HBTs), or lasers [1-5]. Selective area doping is also used in FETs to form precisely controlled channel or lightly doped drain (LDD) regions [6]. Second, implantation is employed to form locally high resistance regions for inter-device isolation such as in integrated FET circuits or for current guiding in lasers [7-12]. Third, ion implantation can be used to promote local area inter-diffusion or mixing of the host atoms to alter the local bulk properties of the semiconductor [13].

In this paper we focus on specific examples of using ion implantation for controlled, selective area doping. We begin by highlighting the key features in achieving high performance ion implanted GaAs Junction Field Effect Transistors (JFETs) that rely on shallow, abrupt p-type doping profiles as well as abrupt channel doping. The utility of heavy ion implantation (Zn and Cd) along with the co-implantation of P will be presented.

In a second area of study, we address the issues associated with implant doping of advanced ternary compound semiconductors materials such as AlGaAs, InGaP, and InAlP that are potential barrier layers for heterostructure field effect transistors (HFETs). The ability to selectively dope these barrier layers will enable improved HFET designs. For AlGaAs we report on a comprehensive study of Si implant doping over a wide Al-compositional range from 0 to 70 %. This enables us to separate fundamental donor ionization effects from implant activation phenomena. The results are explained with a ionization energy and density-of-states treatment that will have application to epitaxial doping as well.

For InGaP and InAlP, we report on the donor saturation level versus Si-implant dose and show that this level can be increased in InGaP by an appropriate P co-implantation scheme. The Si donor ionization level in these phosphide materials is also estimated from variable temperature Hall measurements and compared to that of AlGaAs with a similar bandgap.

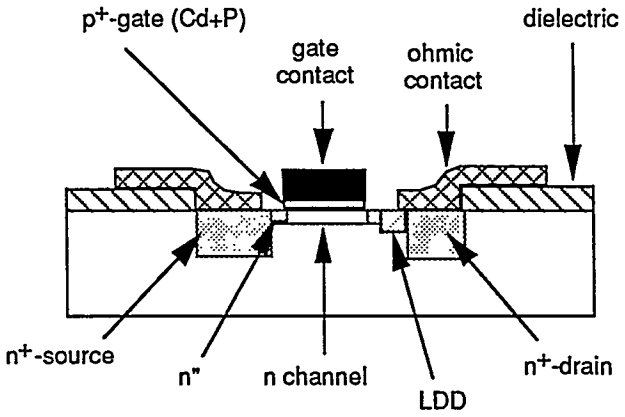

FIG 1. Schematic of all ion implanted, self-aligned, GaAs JFET.

P-TYPE IMPLANTATION DOPING FOR GaAs JFETs

Figure 1 shows a schematic representation of a self-aligned GaAs JFET where all doping is done by ion implantation [5]. This structure overcomes several of the traditional short-comings of non-self-aligned or diffused junction JFETs such as an increased gate-to-source capacitance (C_{GS}) due to the p/n junction gate and gate length broadening during the p^+ gate formation. The attributes of this structure have been well documented elsewhere for devices with gate lengths down to ~0.7 μm [14-16]. To extend this structure to sub-half-micron gate lengths, both the vertical and lateral doping profile must be modified. For the vertical profile, the p^+-gate region must be made very shallow while still maintaining high doping at the surface to insure an ohmic gate contact. The channel profile also becomes more critical at short gate lengths with abrupt doping being required to reduce short channel effects and achieve good carrier confinement. The lateral n-type doping profile must also be modified for short gate operation to minimize hot carrier effects and impact ionization on the drain side of the gate to reduce short channel effects and improve the breakdown voltage. This is accomplished with the use of lightly doped regions on both sides of the gate (n") defined by dielectric sidewall spacers and an additional asymmetric lightly doped region on drain side of the gate (lightly doped drain, LDD). These regions are represented in Fig. 1. In this paper we discuss experimental improvements to the vertical p-type doping profile, in particular, the p^+-gate implant. Optimization of the lateral profile will be presented elsewhere [17].

While initial work on the JFET structure in Fig. 1 employed Mg-implantation to form the p^+-gate region later generations demonstrated the utility of using the a heavier acceptor species such as Zn [15, 18]. That work clearly showed that abrupt, shallow p^+-regions can be formed with Zn-implantation when a P co-implantation is included. The effect of the P co-implantation can be explained via two possible mechanisms, both of which increase the probability of the Zn-ion to occupy the column III sublattice and act as an acceptor [18]. Once the Zn is substitutional on a Ga-site its diffusion coefficient is dramatically reduced compared to the fast diffusing interstitial Zn as exists in an external source Zn-diffusion. The mechanisms both stem from the realization that as-implanted material will consist of both Ga and As vacancies and interstitials due to the radiation damaged introduced in the implantation process. The first possible mechanism is that the P-ion will fill As-vacancies thereby forcing the formation of excess Ga vacancies which the Zn can occupy [19]. Second, the P-ions may tie up interstitial Ga thereby rebuilding the lattice and reducing the competition between the host column III-elements and implanted Zn atoms for occupation of the vacant Ga-sites [20].

The same discussion on the effect of P co-implantation can also be extended to Cd implantation in GaAs. Cd will form still shallower implanted profiles than Zn (for the same energy) due to its heavier mass (120 versus 64 AMU). Figure 2 shows secondary ion mass spectroscopy (SIMS) profiles for the Cd-gate implant (45 keV, $3x10^{14}$ cm^{-2}) either alone or with a P co-implant ($^{62}P_2$: 40 keV, effective ^{31}P dose of $6x10^{14}$ cm^{-2}). The use of P along with Cd is seen to markedly reduce the in-diffusion of Cd. The reduction in diffusion is critical to achieving the required abrupt p/n junction gate. Using a Cd-implanted gate, a p/n junction depth of 35 nm has been demonstrated after the 830 °C activation anneal [16].

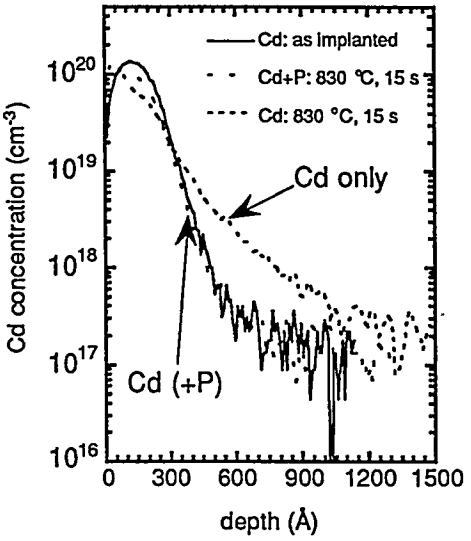

Fig 2. SIMS profiles for Cd as-implanted (45 keV, $3x10^{14}$ cm^{-2}) and annealed (830 °C, 15 s) with and without a P co-implant ($^{62}P_2$: 40 keV, effective P dose of $6x10^{14}$ cm^{-2}). The P co-implantation is seen to dramatically reduce the redistribution of Cd during the anneal.

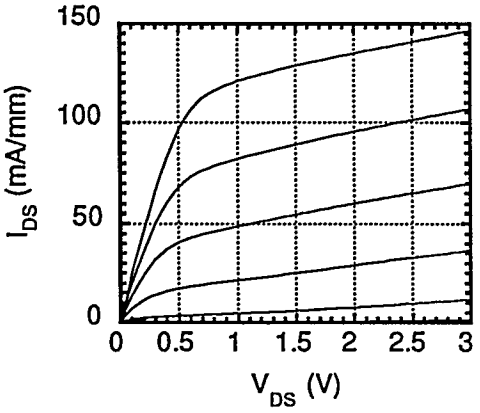

Fig 3: I_{DS} versus V_{DS} for a 0.7 x 50 μm^2 Cd-gate JFET.

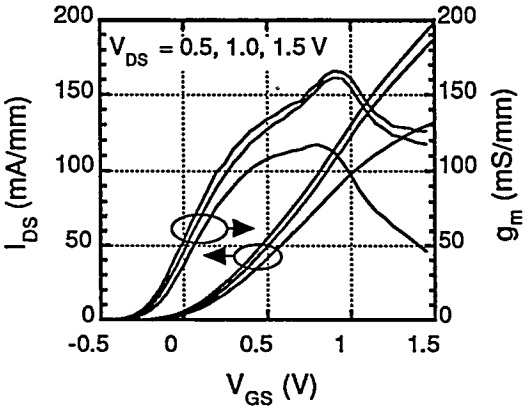

Fig 4: I_{DS} and g_m versus V_{GS} for a 0.7 x 50 μm^2 Cd-gate JFET.

Figure 3 and 4 show the DC performance a 0.7 x 50 μm^2 Cd-gate JFET. A saturation current of 130 mA/mm and transconductance of 165 mS/mm was realized at V_{DS} = 1.5 V and V_{GS} = 1 V. This same device had a unity current cutoff frequency (f_t) of 26 GHz and a maximum oscillation frequency (f_{max}) of 42 Ghz [16]. These frequency metrics are comparable to a similar gate length GaAs MESFET; however, the JFET has a 0.4 to 0.5 V

higher gate turn-on voltage [V_{GS}(on) ~ 1V] than the MESFET [V_{GS}(on) ~ 0.55 V] which will significantly reduce power consumption.

Si-IMPLANTATION IN AlGaAs

500 nm thick undoped AlGaAs layers were grown at 590 °C in a Varian Gen II MBE reactor on semi-insulating (100) GaAs substrates. A 200 nm undoped GaAs buffer was grown prior to the AlGaAs layer and a 5 nm GaAs cap layer was grown on top of the AlGaAs to inhibit oxidation. This MBE system has been used to grow high mobility AlGaAs/GaAs two dimensional electron gas structures with 77 K mobilities in excess of 10^6 cm^2/Vs demonstrating the high quality of the AlGaAs/GaAs material grown in this system [21]. ^{29}Si-implants were performed in a non-channeling direction at an energy of 100 keV at a dose of either $5.6x10^{12}$ or $2.8x10^{13}$ cm^{-2}. These doses are in the range used for FET channel and LDD formation or source/drain formation, respectively. Beam currents were kept below 0.1 $\mu A/cm^2$ to minimize sample heating and in-situ annealing. The estimated ion peak range is at 100 nm from the surface with a corresponding peak concentration of ~$1.8x10^{18}$ cm^{-3} for the higher dose samples. This concentration level is in the range where Si doping starts to saturate in GaAs [22]. Annealing was performed for 15 s in flowing Ar in a SiC coated graphite susceptor that had been precharged with As [23]. Room temperature and variable temperature (T = 77 to 400 K) Hall measurements were done using Van der Pauw Hall samples with In/Sn contacts alloyed at the corners of each sample at 400 °C for 1 min.

Figure 5 shows n_s versus %AlAs for the samples annealed at 900 °C. This temperature was determined to yield a maximum value of n_s for this implant dose. n_s is seen to be relatively constant for a given dose out to 20% AlAs, dramatically decreases at 35% AlAs, and then increases at the higher Al-fractions (50 and 70% AlAs). The reason for these variations will be discussed in more detail shortly.

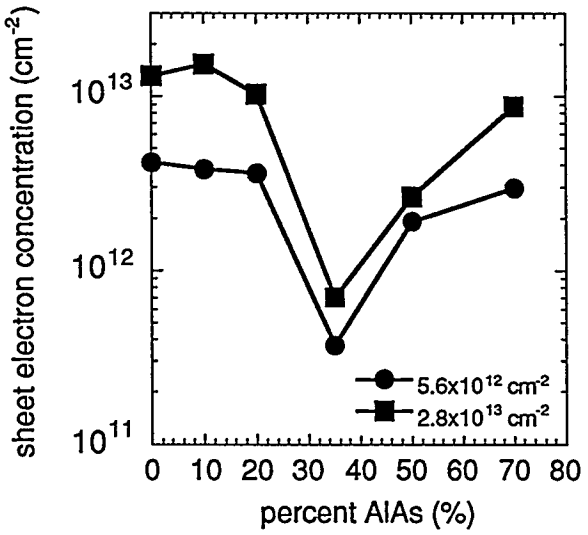

Fig 5. Sheet electron density versus %AlAs for AlGaAs implanted with Si at 100 keV for the two doses shown. The samples were annealed at 900 °C for 15 s.

By doing variable temperature Hall measurements on the high dose sample from Fig. 5, the apparent donor ionization energy (E_d) can be estimated assuming:

$$n_S \propto \exp\left(\frac{-E_d}{kT}\right) \qquad (1)$$

The apparent ionization energy levels are listed in Table I, along with η_{eff}. Our values of E_d agree well with those reported for epitaxial Si-doped AlGaAs [24]. The 35 and 50% samples are seen to have similar ionization energy levels near 160 meV while the 70% sample has two levels at 86 and 55 meV. The two levels in the 70% sample correspond to the deep DX level (86 meV) and the hydrogenic donor level (55 meV) corresponding to different local Al and Ga environments about the Si atoms. For the 35 and 50% samples the free electrons all freeze-out into the deep DX level and the shallow donor level is not seen. Since the ionization energies are similar in the 35 and 50% samples, the ionization energy levels alone do not explain the effective activation efficiency dependence on Al-fraction shown in Fig 5. That is, based solely on the ionization energy, the 35 and 50% samples should both have similarly low activation but this is seen not to be the case from Table I.

Table I: Summary of ionization energies and effective activation efficiency of Si-implanted AlGaAs for the two doses studied.

%AlAs	apparent ionization energy, E_d (meV)	η_{eff}[a] $\phi = 5.6\times10^{12}$ cm^{-2}	η_{eff}[a] $\phi = 2.8\times10^{13}$ cm^{-2}
0	3.2	74.3	46.8
10	4.3	67.9	54.6
20	9.2	64.3	36.8
35	162	6.6	2.5
50	155	34.1	9.5
70	86, 55	52.8	31.1

[a] $\eta_{eff} = (n_S/\phi)\times100$

Figure 6 shows the dependence of the conduction band density-of-states in AlGaAs versus %AlAs based on the expression given below [25]:

$$N_c \equiv 2\left(\frac{2\pi m_{de} kT}{h^2}\right)^{3/2} M_c \qquad (2)$$

where M_c is the number of equivalent minima in the conduction band and m_{de} is the density-of-states effective mass given by

$$m_{de} = (m_e^{\Gamma} m_e^{X} m_e^{L})^{1/3} \qquad (3)$$

where m_e^{Γ}, m_e^{X}, and m_e^{L} are the effective electron mass in each of the energy bands and vary with Al-composition as follows [26]:

$$m_e^{\Gamma} = 0.067 + 0.83x \qquad (4a)$$

$$m_e^{X} = 0.32 - 0.06x \qquad (4b)$$

$$m_e^{L} = 0.11 + 0.03x \qquad (4c)$$

Other terms in Eqn 2 have their usual meaning.

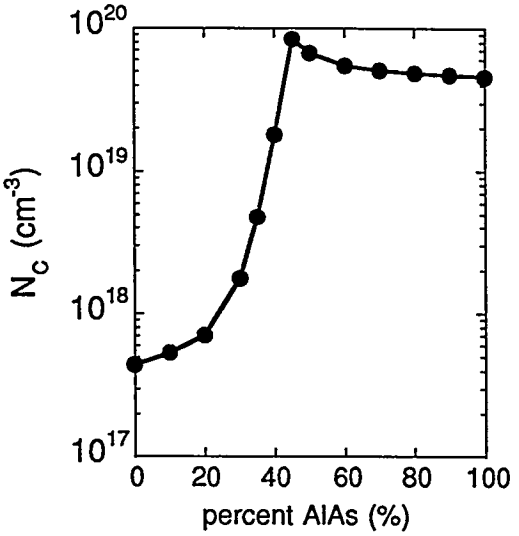

Fig 6. Conduction band density-of-states versus %AlAs for AlGaAs calculated using Eqn 2.

The free electron density (n) can then be expressed as:

$$n = N_c \exp\left(\frac{-(E_c - E_f)}{kT}\right) \tag{5}$$

where E_c is the conduction band minimum energy. The position of the Fermi level (E_f) can be solved for from the following expression for the density of ionized donors:

$$N_d^+ = N_d\left[1 - \frac{1}{1 + \frac{1}{g}\exp\left(\frac{E_d - E_f}{kT}\right)}\right] \tag{6}$$

assuming the implanted layer thickness is equal to two standard deviations of the profile (t_{imp} = two implant straggles = $2\Delta R_p$) and N_d = (implanted dose)/t_{imp} . g is the electron ground state degeneracy and is equal to 2. E_d is the donor ionization energy listed in Table I. We further assume $N_d >> N_a$ and take the density of ionized donors to be equal to the measured sheet electron concentration divided by t_{imp}.

Figure 7 is a plot of calculated n from Eqn 5 and measured n ($n=n_s/t_{imp}$) versus %AlAs for the high dose samples at 300 K. The trend of electron concentration versus %AlAs, particularly the pronounced minima at 35% AlAs, is consistent between the calculated values and measured data. However, the lack of absolute agreement between the theory and experiment is up to an order-of-magnitude and has several possible origins. First, as already stated, Eqn 5 is only an approximation that does not account for compensation effects. Second, previous work on epitaxial AlGaAs has shown the difficulty in achieving absolute agreement between a theoretical density-of-states treatment of electron concentrations and the measured Hall concentration even when a full charge balance description is employed that includes acceptor compensation [27]. In that work a difference of an order-of-magnitude was reported between theory and Hall data. The lack of agreement is likely the result of the complex band structure of AlGaAs. Third, the 0, 10 and 20% samples will be degenerately doped since N_c is only ~7×10^{17} cm^{-3} at 20% AlAs. Therefore, Eqn 6 does not yield the correct Fermi level position. Fourth, for implanted material several additional factors can be expected to affect the electron profile. For example, since the electron distribution is not uniform the mobility and compensation ratio is expected to vary throughout the profile. The Hall measurement also will only yield an average value for electron concentration and mobility that

at best can be treated with a two band conduction model but in practice is not readily separated into its component parts. Finally, the defects generated during the implantation process which can act as either compensating acceptors or as scattering centers that degrade the electron mobility are most likely not the same in the different Al composition samples. Therefore, it is not clear that assuming a set compensation ratio over the entire compositional range is valid or useful.

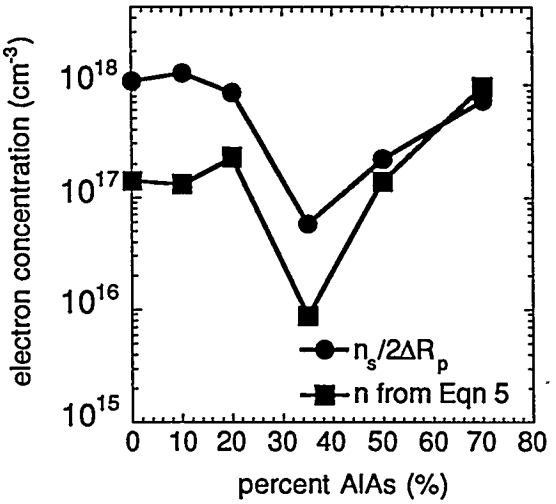

Fig 7. Calculated (based on Eqns 5 and 6) and measured electron concentration versus %AlAs for AlGaAs implanted with Si at an energy of 100 keV and a dose of 2.8×10^{13} cm^{-2}.

Despite the shortcomings to the theory just discussed, the general variation in electron concentration evident in Fig. 5 can be qualitatively explained by the combined ionization energy and density-of-states treatment. We feel this treatment, although not absolute, is the most appropriate approach for explaining the Si-implantation results in AlGaAs.

Si AND Si+P IMPLANTATION IN InGaP AND InAlP

We now turn to Si-implantation doping of InGaP and InAlP. $In_{0.5}Ga_{0.5}P$ and $In_{0.5}Al_{0.5}P$ epitaxial layers lattice matched to GaAs have been employed as replacement materials for AlGaAs in semiconductor lasers, heterojunction bipolar transistors (HBTs), and heterostructure field effect transistors (HFETs) [28-32]. InGaP is of interest because it does not suffer from the deep donor (DX) level associated with Al-containing materials while InAlP (E_g = 2.3 eV for x=0.5) is attractive due to its higher bandgap than $Al_xGa_{1-x}As$, even for x=1 [30,33].While initial work in these materials focused mostly an laser and HBT applications, recent progress has been made in HFETs [34]. While HFETs are particularly suited to the application of ion implantation doping to reduce the device access resistance, there are a limited number of reports on ion implantation doping of InGaP and InAlP. Ion implantation doping of these materials can be expect to play an enabling role in advanced transistor designs as has been the case for more mature semiconductor technologies based on Si and GaAs. Although n-type ion implantation doping of InGaP [35] and InAlP [36] with Si has been reported, further work is needed to optimize Si-implantation in these materials.

$In_{0.5}Ga_{0.5}P$, $In_{0.5}Al_{0.5}P$, and $In_{0.5}Ga_{0.25}Al_{0.25}P$ layers were grown at 640 °C by metalorganic chemical vapor deposition (MOCVD) on (100) semi-insulating GaAs in an Emcore rotating disk reactor. The source gases were trimethylgallium, trimethlyindium, arsine, and phosphine. X-ray measurements confirmed that the films were lattice matched to the GaAs substrate within 0.22% for InGaP and 0.4% for the Al-containing films. ^{29}Si implants were performed in a nonchanneling direction at 90 keV at one of four doses (1, 5, 10, or 50×10^{13} cm^{-2}). P co-implants were done at 100 keV to overlay the Si-profile and at five multiples of the Si-dose (0, 0.5, 1.0, 1.5, or 2.0). After implantation, samples were annealed

in a SiC coated graphite susceptor in flowing Ar for 15 s at the prescribed temperature ± 5°C. Prior to heating a three cycle pump/purge sequence is employed to reduce background oxygen levels. Room temperature and variable temperature Hall measurements were performed in a van der Pauw configuration with In/Sn or In/Pb contacts alloyed at the corners of the samples at 400 °C for 1 min.

Figure 8 shows the sheet electron concentration (n_s) versus annealing temperature for Si-implanted InGaP at four doses. n_s is seen to reach a maximum value of $1.33x10^{13}$ cm^{-2} in the range of 850 to 900 °C for a dose of $5x10^{13}$ cm^{-2} which is consistent with the earlier results of Si-implanted InGaP [35]. At higher doses self compensation starts to occur as Si demonstrates an amphoteric behavior. As will be demonstrated next, this saturation level can be increased by the application of P co-implantation.

Figure 9 shows the sheet electron concentration (n_s) versus annealing temperature for Si-implanted InAlP at three doses (5, 10, or $50x10^{13}$ cm^{-2}). InGaAlP implanted at a dose of $5x10^{13}$ cm^{-2} had n_s values after annealing almost identical to the same dose InAlP samples. For the lowest dose the samples were highly resistive for annealing temperatures below 750 °C and then display less than 4% effective activation out to 900 °C. n_s in the higher dose InAlP samples continues to increase out to 900 °C to a maximum of $9.6x10^{12}$ cm^{-2} but still with an effective activation efficiency of only ~10%. The lack of data for the lowest dose samples below 850 °C results from the difficulty in forming reliable Hall contacts to these high resistance samples.

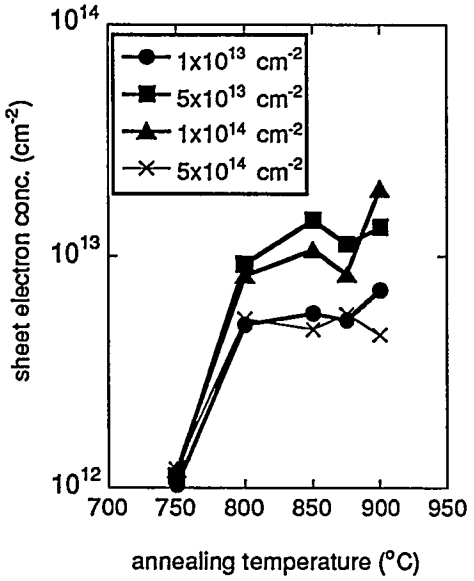

Fig 8. Sheet electron concentration versus annealing temperature for 90 keV Si-implanted InGaP at the doses shown.

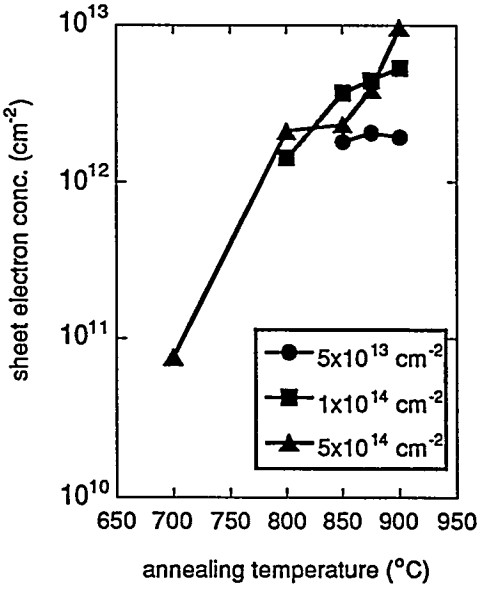

Fig 9. Sheet electron concentration versus annealing temperature for 90 keV Si-implanted InAlP at the doses shown.

Figure 10 shows the change in n_s versus P co-implantation dose normalized to the Si-dose for two Si-doses in InGaP and one dose in InAlP. These samples were all annealed at 900 °C for 15 s. Although n_s of the low dose InGaP samples does not change significantly with P co-implantation over the P-dose range studied, the InGaP material implanted with a dose of $5x10^{13}$ cm^{-2} demonstrates a dramatic increase in n_s for a P dose of $2.5x10^{13}$ cm^{-2} (0.5 times the Si-dose) while the InAlP shows an increase for a P-dose 1.5 times the Si-dose. The InAlP sample with 1.5xP has a 35% increase in n_s but this still only corresponds to ~5% effective activation efficiency. The reason for this low activation will be addressed later.. The

InGaP sample with 0.5xP has a 65% increase in n_s from the sample without P which corresponds to 44% activation in the co-implant sample. The decrease in n_s at higher P-doses can be explained by local deviation of stoichiometry due to excess P or to the additional implant damage not being completely removed at the higher doses. The increase in n_s at 0.5xP corresponds to a 41% reduction in the sheet resistance from 530 to 310 Ω/□. Such a reduction will have a dramatic effect on the performance of a FET that incorporates a InGaP barrier layer and Si-implantation doping in the source and drain regions. The improvements seen here for n_s in InGaP are slightly higher than that seen for Si/P implants in GaAs (~50%) [37] and InP (~30%) [38].

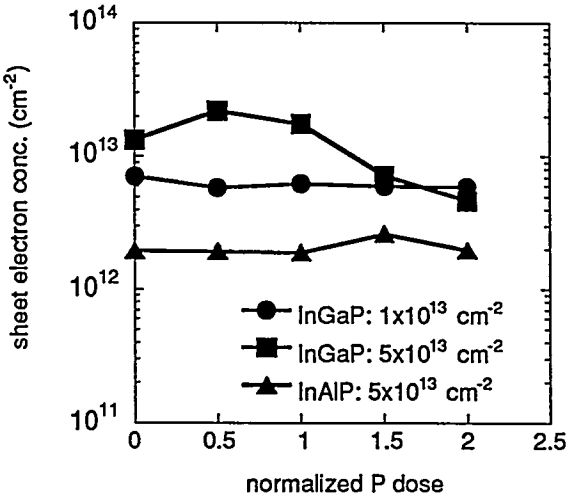

Fig 10. Sheet electron concentration versus P co-implant dose normalized to the Si-implant doses listed for InGaP and InAlP. The samples where annealed at 900 °C for 15 s.

The effect of the P co-implantation can be explained via the same two possible mechanisms discussed above for P co-implants with Zn or Cd with the additional consideration of three host elements. In addition, since the host elements of InGaP and InAlP have significantly different atomic masses, as compared to GaAs where the elements are similar, local stiochiometry variations will exist in the crystal after implantation due to the different amount of recoil of each element. The P-implantation will therefore also help to restore the local crystal stiochiometry.

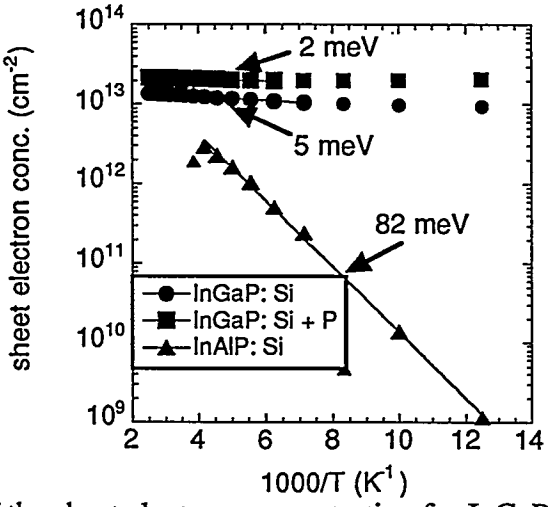

Fig 11. Arrhenius plot of the sheet electron concentration for InGaP implanted with Si-only or with Si+P(0.5xSi) and InAlP implanted with Si-only. The Si dose is $5x10^{13}$ cm^{-2}. The estimated donor ionization energies are listed on the figure.

Finally, the Si-donor apparent ionization energies were estimated from the Arrhenius plot in Fig. 11 for InGaP and InAlP. Both the InGaP implanted with Si-only and Si+P are seen to have shallow donor levels in the range of 2-5 meV. In contrast, the InAlP sample has an estimated ionization energy level of ~80 meV that will limit the number of ionized donors at room temperature to ~4.5% of the active Si-donors. This means the Si/1.5xP InAlP sample in Fig. 10 has effectively 100% Si-activation on column III sites but with only ~5% ionized donors at room temperature. The results for InGaP are particularly important when compared to Si-implanted AlGaAs with the same energy gap at 35% AlAs. Si-implantation in $Al_{0.35}Ga_{0.64}As$ is limited by the high donor ionization energy (~160 meV) associated with the DX level and relatively low conduction band density-of-state at this composition [39]. Therefore, InGaP is extremely attractive as an alternative to AlGaAs in n-type doped structures whether they are formed by implantation or epitaxially grown due to the shallow donor level. InAlP, on the other hand, will behave more like AlGaAs, although with a somewhat shallower donor level.

CONCLUSION

In conclusion, we have presented results on Cd-implantation in GaAs to achieve very shallow p^+-regions for short gate JFETs. Using this approach junction depths of 35 nm have been achieved. A comprehensive study of Si-implantation doping in AlGaAs was also presented with the results explained based on the ionization energy and the conduction band density-of-states dependence on Al-composition. This treatment qualitatively explains why a strong minima is seen at 35% AlAs in the measured electron density. Finally, we have reported on the activation properties of Si-implanted InGaP and InAlP. An optimum dose P co-implantation was shown to increase the donor saturation level by 65% in InGaP and 35% in InAlP. The Si-donor ionization level was shown to be very shallow in InGaP while it is estimated to be ~80 meV in InAlP due to the existence of a DX level. This work improves the understand of ion implantation doping in these materials and will enable continued advances in ion implanted compound semiconductor devices.

Acknowledgment:

The authors gratefully acknowledge J. Escobedo for assistance with rapid thermal annealing and ion implantation, the expert device processing of G. Lopez, and the technical support of T. Henson and J. Avery with Hall characterization. The work was supported by the Department of Energy under contract #DE-ACO4-94AL85000.

REFERENCES

[1] K. Daoud-Ketata, C. Dubon-Chevallier, and C. Besombes, IEEE Trans. Elec. Dev. **8**, 205 (1987).
[2] S. J. Pearton, F. Ren, P. W. Wisk, T. R. Fullowan, R. F. Kopf, J.-M. Kuo, W. S. Hobson, and C. R. Abernathy, J. Appl. Phys. **62**, 698 (1991).
[3] J. P. de Souza and D. K. Sadana, IEEE Trans. Elec. Dev. **39**, 166 (1992).
[4] M. Feng and J. Laskar, IEEE Trans. Elec. Dev. **40**, 9 (1993).
[5] J. C. Zolper, A. G. Baca, R. J. Shul, A. J. Howard, D. J. Rieger, M. E. Sherwin, M. L. Lovejoy, H. P. Hjalmarson, B. L. Draper, J. F. Klem, and V. M. Hietala, IEEE Trans. Elec. Dev, **41**, 1078 (1994).
[6] A. I. Akinwanda, K. L. Tan, C. H. Chen, and P. J. Vold, IEEE Elec. Dev. Lett. **9**, 275 (1988).
[7] D. C. D'Avanzo, IEEE Trans. Elec. Dev. **29**, 1051 (1982).
[8] F. Ren, S. J. Pearton, W. S. Hobson, T. R. Fullowan, J. Lothian, and A. W. Yanof, Appl. Phys. Lett. **56**, 860 (1990).
[9] J. C. Zolper, A. G. Baca, and S. A. Chalmers, Appl. Phys. Lett. **62**, 2536 (1993).
[10] S. J. Pearton, Mat. Sci. Rep. **4**, 313 (1990).

[11] M. Orenstein, N. G. Stoffel, A. C. Von Lehmen, J. P. Harbiunson, and L. T. Florez, Appl. Phys. Lett. **59**, 31 (1991).
[12] K. L. Lear, R. P. Schneider, K. D. Choquette, S. P. Kilcoyne, J. J. Figiel, and J. C. Zolper, IEEE Photonic Tech. Lett. **6**, 1053 (1994).
[13] D. G. Deppe and N. Holonyak, Jr. J. Appl. Phys. **64**, R93 (1988).
[14] J. C. Zolper, M. E. Sherwin, A. G. Baca, R. J. Shul, J. F. Klem, and V. M. Hietala, IEEE Elec. Dev. Lett. **15**, 493 (1994).
[15] M. E. Sherwin, J. C. Zolper, A. G. Baca, R. J. Shul, A. J. Howard, D. J. Rieger, J. F. Klem, and V. M. Hietala, IEEE Elec. Dev. Lett. **15**, 242 (1994).
[16] J. C. Zolper, A. G. Baca, M. E. Sherwin, and R. J. Shul, Elec. Lett. **31**, 923 (1995).
[17] J. C. Zolper, A. G. Baca, V. M. Hietala, R. J. Shul, and M. E. Sherwin, submitted to Device Research Conf. 6/96.
[18] M. E. Sherwin, J. C. Zolper, A. G. Baca, T. J. Drummond, R. J. Shul, A. J. Howard, D. J. Rieger, R. P. Schnieder, and J. F. Klem, J. Elec. Mater. **23**, 809 (1994).
[19] G. Landgren and W. H. van Berlo, J. Appl. Phys. **63**, 2783 (1989).
[20] K. K. Patel and B. J. Sealy, Appl. Phys. Lett. **48**, 1467 (1986).
[21] J. F. Klem, private communication.
[22] S. J. Pearton, J. Mod. Phys. B **7**, 4687 (1993).
[23] S. J. Pearton, A. Katz, and M. Geva, J. Appl. Phys. **68**, 2482 (1990).
[24] N. Chand, T. Henderson, J. Klem, W. T. Masselink, R. Fisher, Y. C. Chang, and H. Morkoç, Phys. Rev. B **30**, 4481 (1984).
[25] S. M. Sze, Physics of Semiconductor Devices, 2nd edition, (John Wiley, New York, NY, 1981) pp. 17- 24.
[26] S. Adachi, J. Appl. Phys. **58**, R1 (1985).
[27] S. P. Svensson and A. W. Swanson, J. Appl. Phys. **59**, 2870 (1986).
[28] H. Asahi, Y. Kawamura, and H. Nagai, J. Appl. Phys. **54**, 6958 (1983).
[29] K. Kobayashi, I. Hino, A. Gomyo, S. Kawata, and T. Suzuki, IEEE J. Quantum Electron. **23**, 704 (1987).
[30] J. H. Quigley, M. J. Hafich, H. Y. Lee, R. E. Stave, and G. Y. Robinson, J. Vac. Sci. Technolo. B **7**, 358 (1989).
[31] D. P. Bour, J. R. Shealy, G. W. Wisks, and W. J. Schaff. Appl. Phys. Lett. **50**, 615 (1987).
[32] J. S. Yuan, M. T. Tsai, C. H. Chen, R. M. Cohen, and G. B. Stringfellow, J. Appl. Phys. **60**, 1346 (1986).
[33] S. Adachi, J. Appl. Phys. **63**, 64 (1988).
[34] K. Wantanabe, F. Hyuga, H. Yamazaki, and T. Nittono, J. Appl. Phys. **78**, 5939 (1995).
[35] S. J. Pearton, J. M. Kuo, F. Ren, A. Katz, and A. P. Perley, Appl. Phys. Lett. **59**, 1467 (1991).
[36] S. J. Pearton, W. S. Hobson, J. M. Kuo, H. S. Luftman, A. Katz, and F. Ren, Appl. Phys. Lett. **60**, 1117 (1992).
[37] F. Hyuga, H. Yamazaki, K. Wanatabe, and J. Osaka, Appl. Phys. Lett. **50**, 1592 (1987).
[38] A. Dodabalapur and B. G. Streetman, J. Elec. Mat. **18**, 65 (1989).
[39] J. C. Zolper, J. F. Klem, A. G. Baca, M. E. Sherwin, M. J. Hafich, and T. J. Drummond, J. Appl. Phys., submitted 2/96.

DISCLAIMER